Implications of How the Linewidth Enhancement Factor is Introduced on the Lang and Kobayashi Model

C. Masoller

***Abstract*—The implications of how the linewidth enhancement factor is introduced on the Lang and Kobayashi model of a single-mode semiconductor laser with optical feedback are numerically investigated. α is introduced on the model in the rate equation for the complex electric field by performing an expansion of the frequency of the laser mode around its threshold value ω_o. Two different expansions of have led to two different sets of Lang and Kobayashi equations; in the first set, the intensity reduction of the optical gain G is taken into account in the linearization of ω, while in the second set it is neglected. Although in the literature the investigations of semiconductor lasers with optical feedback have been based on either of these sets, they are equal only when a linear form for G is assumed. In this paper, it is shown that on which set of Lang and Kobayashi equations the investigations are based is an important fact to take into account when interpreting the results, since it is shown that if the nonlinear gain is considered, the dynamics predicted by the two sets are very different. In particular, it is shown that behavior of the external cavity modes and the stability properties of the attractors differ greatly when the gain saturation coefficient ε is varied.**

I. Introduction

In SEMICONDUCTOR lasers, the carrier density dependence of the refractive index plays a fundamental role, since it introduces a coupling between the amplitude and the phase fluctuations of the electric field. The coupling is basically caused by the fact that a change in the real part of the susceptibility (proportional to the refractive index) will be accompanied by a change in the imaginary part of the susceptibility (proportional to the gain) via the Kramers–Kroning relations. The coupling is described by the linewidth enhancement factor [1]

$$\alpha = -2k_o \frac{\Delta n'}{\Delta g} \tag{1}$$

where k_o is the free-space wave vector and $\Delta n'(\Delta g)$ is the change in the real part of the refractive index (in the electronic gain per length) occurring when the carrier density is altered.

α is one of the fundamental parameters for semiconductor lasers. It is responsible for the enhancement of the laser linewidth, affects the frequency chirp, the modulation response, the injection-locking range, and the effect of external feedback [2].

Optical feedback in semiconductor lasers has attracted the attention of many researchers owing to its practical importance as well as to the rich variety of nonlinear behavior observed. It is well known that a small amount of feedback can be useful for linewidth reduction, but the feedback intensities that are likely to occur in optical communication systems can lead to the occurrence of "coherence collapse," in which the laser linewidth is enhanced from a few megahertz to several gigahertz.

The theoretical studies of semiconductor lasers with external feedback are commonly based on the Lang and Kobayashi model [3], which has proven to give a detailed understanding of the observed laser characteristics, such as noise properties, linewidth reduction, stability properties, spectral behavior, and the onset of coherence collapse [4]–[9].

The model consists of rate equations for the complex electric field and for the carrier density inside the laser cavity. The field equation is the standard laser equation plus a single time-delayed term that takes into account the field reflected from the external cavity (since multiple reflections are neglected, the model is valid for low to moderated feedback levels). Assuming the laser oscillates in a single longitudinal mode with threshold frequency ω_o, and writing the complex electric field as $E(t)\exp[i(\omega_o t + \phi(t))]$, the deterministic equations that were originally introduced by Lang and Kobayashi are

$$\frac{d[E(t)e^{i\phi(t)}]}{dt} = \left[i(\omega - \omega_o) + \frac{1}{2}\left(G - \frac{1}{\tau_p}\right)\right]E(t)e^{i\phi(t)} + \frac{k}{\tau_{\text{in}}}E(t-\tau)e^{i\phi(t-\tau)}e^{-i\omega_o\tau} \tag{2}$$

$$\frac{dN(t)}{dt} = J - \frac{N(t)}{\tau_s} - GE(t)^2 \tag{3}$$

where ω is the frequency of the longitudinal mode, $\tau = 2L_{\text{ext}}/c$ is the round-trip time of the light in the external cavity of length $L_{\text{ext}}, \tau_{\text{in}}$ is the round-trip time in the laser cavity, τ_p is the photon lifetime, and τ_s is the carrier lifetime. The field amplitude $E(t)$ is normalized such that $I = VE^2$ is the total photon number in the laser waveguide (V being the volume of the active region). k is the feedback parameter, and J is the current density.

Manuscript received June 7, 1996; revised December 3, 1996. This work was supported by Project 47 of the BID-CONICYT Program of the Consejo Nacional de Ciencia y Tecnologia (CONICYT).of Uruguay, the Comision Sectorial de Investigacion Cientifica (CSIC) and the PEDECIBA.

The author is with the Facultad de Ciencias, Instituto de Física, Universidad de la República, Montevideo, Uruguay.

Publisher Item Identifier S 0018-9197(97)03040-6.

G is the modal gain per unit time ($G = v_g g$, where v_g is the group velocity). The intensity reduction of the gain, which results from spatial and spectral hole burning and carrier heating, is included phenomenologically in the rate equations (2) and (3) by writing G in the form $G = G_o(1-\varepsilon E^2)$, where G_o is the linear gain $G_o = G_N(N - N_o)$ (G_N and N_o being constants), and ε is the gain saturation coefficient.

α is introduced on the model by linearizing ω around its threshold value $\omega_o = \omega(N_{\rm th})$, where $N_{\rm th}$ is the threshold carrier density (which in the absence of feedback is determined by $G(N_{\rm th}) = 1/\tau_p$). The frequency of the laser cavity mode depends on the refractive index and is given by $\omega = p\pi c/n'l$, where c is the velocity of the light, l is the diode cavity length, and p an integer number. Thus, linearizing around threshold conditions and using (1), ω can be written in terms of the α parameter as

$$\omega = \omega_o + \tfrac{1}{2}\alpha\Delta G. \tag{4}$$

In the literature, two different expansions of ΔG in (4) have led to two different equations for the complex electric field. Writing ω as $\omega = \omega_o + 1/2\alpha[G - G(N_{\rm th}] = \omega_o + 1/2\alpha(G - 1/\tau_p)$ and substituting in (2) yields

$$\frac{d[E(t)e^{i\phi(t)}]}{dt} = \left(\frac{1+i\alpha}{2}\right)\left(G - \frac{1}{\tau_p}\right)E(t)e^{i\phi(t)} + \frac{k}{\tau_{\rm in}}E(t-\tau)e^{i\phi(t-\tau)}e^{-i\omega_o\tau}. \tag{5}$$

Since the intensity dependence of the α parameter is not well known, the intensity dependence of G in (4) has been neglected [9]. Therefore, writing ω as [8] $\omega = \omega_o + 1/2\alpha(\partial G/\partial N)|_{N=N_{\rm th}}\Delta N = \omega_o + 1/2\alpha G_N(N - N_{\rm th})$ and substituting in (2) yields

$$\frac{d[E(t)e^{i\phi(t)}]}{dt} = \left[\frac{i\alpha}{2}G_N(N-N_{\rm th}) + \frac{1}{2}\left(G - \frac{1}{\tau_p}\right)\right]E(t)e^{i\phi(t)} + \frac{k}{\tau_{\rm in}}E(t-\tau)e^{i\phi(t-\tau)}e^{-i\omega_o\tau}. \tag{6}$$

The complete system of equations is obtained by combining (5) or (6) with the rate equation for the carrier density (3). These equations have succeeded in explaining week feedback effects in laser diodes and have been studied by several groups [9]–[16].

Equations (5) and (6) are equal only when a linear form for G is assumed. The aim of this paper is to determine whether or not set of equations (5) and (3) (we will refer to this set as set 1) and set of equations (6) and (3) (set 2) predict the same dynamic response of the laser when gain nonlinearities are taken into account.

By numerically integrating the two sets with the same initial conditions and parameters, and varying the parameters k and ε, we show that although when $\varepsilon = 0$ the two sets trivially give the same results, when $\varepsilon \neq 0$, the behavior of the external cavity modes (which are the stationary solutions of the rate equations), the stability properties of the attractors, and the effect of the parameter ε in the dynamics of set 1 are very different from those in the dynamics of set 2. Therefore, the main conclusion of our study is that even for low values of ε set of rate equations on which the investigations are based plays an important role in the results obtained.

This paper is organized as follows. Section II presents the numerical results and analyses of the attractors found when sets 1 and 2 are integrated. In Section III, we study the behavior of the external cavity modes of sets 1 and 2 when ε varies. Finally, Section IV summarizes our conclusions.

II. Results

In this section, we numerically integrate, with the same initial conditions and parameters, sets 1 [(5) and (3)] and 2 [(6) and (3)]. We will show that even for very low values of ε the results obtained from them can be different.

In the numerical simulation, the values adopted for the parameters are $\alpha = 6, G_N = 1.1 \times 10^{-12}$ m^3/s, $N_o = 1.1 \times 10^{24}$ m^{-3}, $\tau_s = 2$ ns, $\tau_p = 2$ ps, $\tau_{\rm in} = 8$ ps, $\tau = 2$ ns, $\omega_o\tau = \pi/2, J = 2J_{\rm th}$ ($J_{\rm th}$ being the threshold current density). The feedback level k and the gain saturation coefficient ε are the free parameters of our study (in order to clarify the exposition of the results, ε is measured in units of 7.5×10^{-24} m^3).

Sets 1 and 2 are integrated with the same Runge–Kutta method and the same initial conditions, which are chosen in the external cavity modes of the laser (i.e., in the stationary solutions of the rate equations). If we neglect the contribution from nonlinear gain, sets 1 and 2 have the same stationary solutions that, written in the form $E^2(t) = I_s, \phi(t) = (\omega_s - \omega_o)t$, and $N(t) = N_s$, satisfy [4], [9]

$$\omega_s\tau - \omega_o\tau = -\gamma\tau[\alpha\cos(\omega_s\tau) + \sin(\omega_s\tau)] = -\gamma\tau\sqrt{1+\alpha^2}\sin(\omega_s\tau + \arctan\alpha) \tag{7}$$

$$G_s = 1/\tau_p - 2\gamma\cos(\omega_s\tau) \tag{8}$$

$$J - N_s/\tau_s - G_s I_s = 0 \tag{9}$$

where $G_s = G_N(N_s - N_o)$ and γ. The modes are obtained by first solving the phase condition (7) for $\omega_s\tau$, which may have multiple solutions, corresponding to multiple external cavity modes. The values of I_s and N_s of a given mode are then calculated from (8) and (9).

Since the value of $\gamma\tau\sqrt{1+\alpha^2}$ determines the amplitude of the sine term of (7), the number of solutions will increase as the feedback increases. A small-signal analysis shows that, for low values of k, only one mode exists and is stable (we will refer to this mode as the perturbed laser mode or mode A), and that as k increases, pairs of modes are created in saddle-node bifurcations. One mode is initially stable (we will refer to this mode as a compound cavity mode) while the other mode is unstable of saddle type (we will refer to this mode as an antimode [9]). For example, for our parameter values and $k = 0.006$, (7) has seven solutions, one corresponds to the perturbed laser mode, three to compound cavity modes, and three to antimodes.

Also, neglecting nonlinear gain effects, we have shown [17] that as k increases, the initially stable modes undergo a quasi-periodic route, and each mode gives rise to periodic oscillations (i.e., a limit cycle) and quasi-periodic oscillations

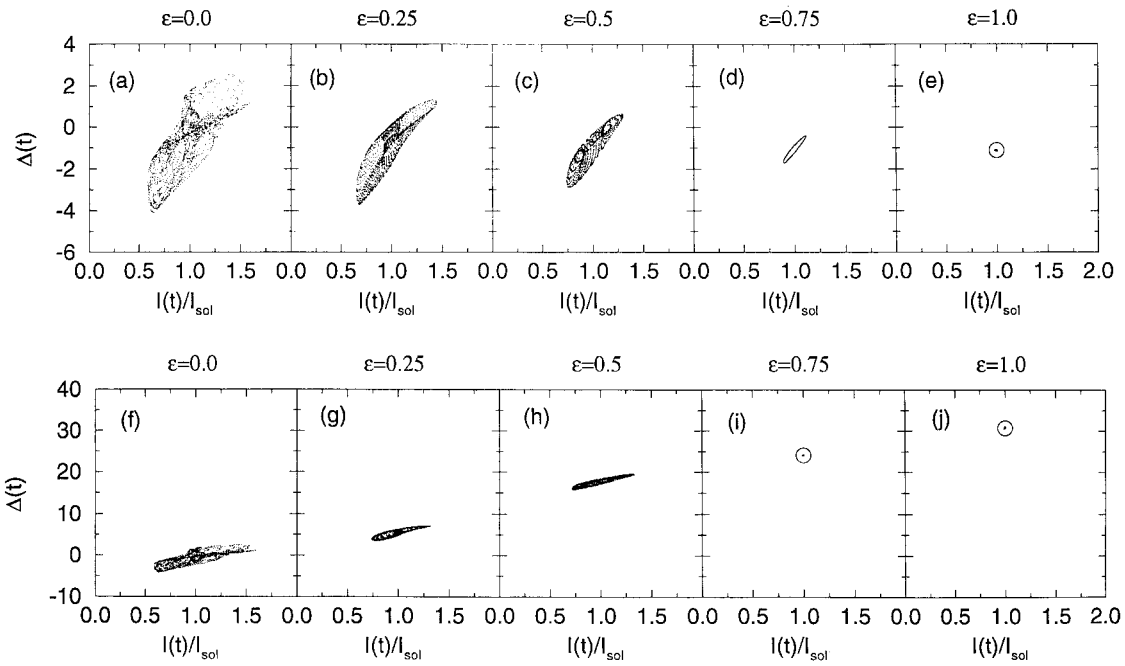

Fig. 1. Trajectories obtained from the numerical simulation of set 1 (first row) and from set 2 (second row). The initial conditions are chosen in mode A for $\varepsilon = 0$, and the evolution of the attractor originated from this mode is studied for $k = 0.0062$ and increasing (ε is measured in units of 7.5×10^{-24} m^3).

(i.e., a torus). As the feedback level continues to increase, the torus become chaotic and eventually lose stability, and the trajectory switches randomly among them.

Let us now show how these results change when the nonlinear gain is taken into account and how they depend on set of rate equations employed in the numerical simulation.

We begin by visualizing the dynamics with phase portraits. We project the trajectory, after a certain number of round trips to eliminate transient effects, in the plane formed by the normalized intensity $I(t)/I_{\rm sol}$ and the phase difference $\Delta(t) = \omega_o\tau + \phi(t) - \phi(t-\tau)$ (since the instantaneous optical angular frequency $\omega(t)$ is given by $\omega = \omega_o + d\phi(t)/dt, \Delta/\tau$ is the optical frequency averaged a round-trip time τ).

Figs. 1 and 2 show the differences between the dynamics predicted by sets 1 and 2, when the parameter is increased from $\varepsilon = 0$ to $\varepsilon = 1$. The first row of the figures shows the results of integrating set 1, while the second row shows the results of integrating set 2. The feedback level was set to $k = 0.0062$ in Fig. 1 and to $k = 0.0072$ in Fig. 2. In the two figures, the numerical simulation was started for $\varepsilon = 0$, and the initial conditions were chosen in the perturbed laser mode w.hich for $\varepsilon = 0$ satisfies (7)–(9)]. The evolution of the attractor originated from this mode was then studied for increasing ε.

Although it is not evident from the figures (the vertical scales of Fig. 2(a)–(e) and (f)–(j) are different), the attractor shown in Fig. 1(a) is equal to the attractor shown in Fig. 1(f), and the attractor shown in Fig. 2(a) is equal to the attractor shown in Fig. 2(f). This is a trivial result, since sets 1 and 2 are equal when $\varepsilon = 0$. Clearly, when $\varepsilon \neq 0$, the results obtained integrating set 1 differ greatly from those obtained integrating set 2.

When the numerical simulation is based on set 1, the phase portraits shown in the first row of Fig. 1 indicate that an increase of the parameter ε causes the attractor to reverse the route to chaos that followed for increasing feedback. The attractor shown in Fig. 1(a) $(k = 0.0062, \varepsilon = 0)$ has a very complicated appearance and was originated from a quasi-periodic route of mode A (we will refer to this attractor as attractor A). Attractor A reverses the route as ε is increased and is a simple torus in Fig. 1(b) and (c), then a limit cycle in Fig. 1(d), and finally a stable mode (indicated with a circle) in Fig. 1(e).

When the numerical simulation is based on set 2, the phase portraits shown in the second row of Fig. 1 indicate that an increase of ε not only causes the attractor to reverse the route to chaos, but it also causes the attractor to have a phase difference Δ that increases with ε.

The same results are found for $k = 0.0072$. For $\varepsilon = 0$ [Fig. 2(a)], the trajectory switches randomly between two unstable attractors: A and B. Attractor B is the attractor originated from the first compound cavity mode (or mode B). Notice that while attractor A has $\Delta < 0$, attractor B has $\Delta > 0$ (mode A has, for the parameter values of Fig. 2, $\omega_s\tau = \Delta \approx -1$, while mode B has $\omega_s\tau = \Delta \approx 4.5$).

When the numerical simulation is based on set 1, an increase of ε causes attractor B to regain stability [in Fig. 2(b), we can see that for $\varepsilon = 0.25$ attractor B is a complicated torus]. However, attractor A also recovers its stability as ε increases. Therefore, when ε is increased from $\varepsilon = 0$ to $\varepsilon = 0.25$ in the numerical simulation, the trajectory obtained will be in attractor A or in attractor B depending on where the trajectory was before the value of ε was increased. The first row of Fig. 2 shows that further increase of ε causes attractor B to reverse the route and to become a limit cycle for $\varepsilon = 1$.

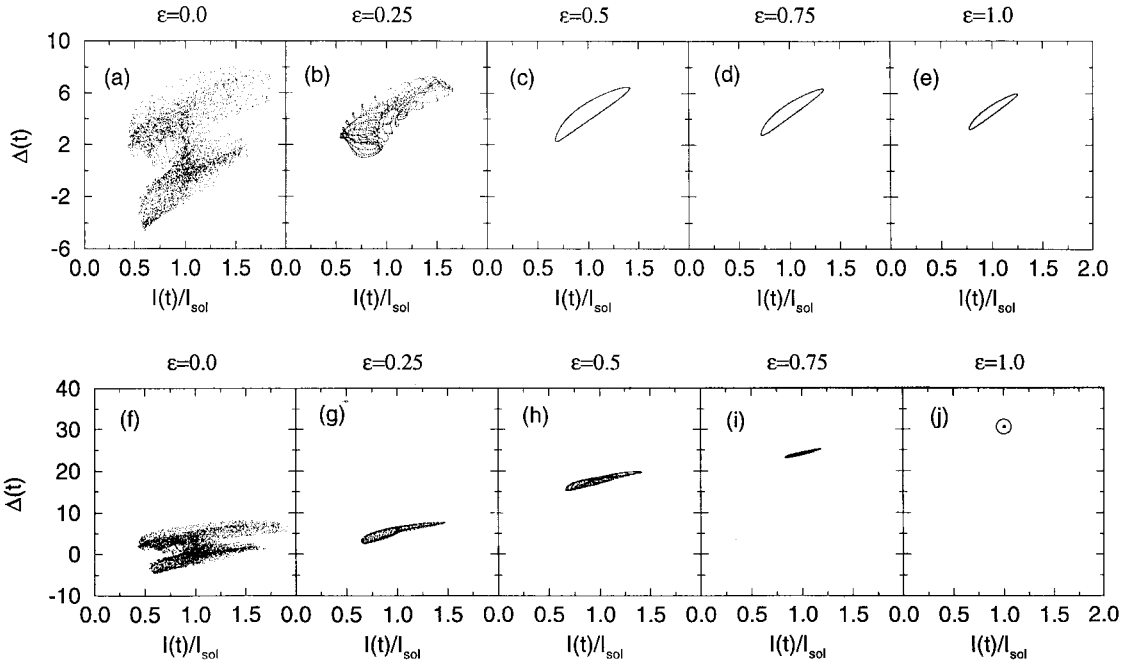

Fig. 2. Phase portraits for $k = 0.0072$ and increasing ε. (a)–(e) show the results of integrating set 1, while (f)–(j) show the results of integrating set 2.

When the numerical simulation is based on set 2, the phase portraits shown in the second row of Fig. 2 demonstrate that an increase of ε, in addition to causing attractor B to become stable and to reverse its route, also causes the attractor to have a phase difference Δ that increases with ε.

Even for very low values of ε, the set of rate equations employed in the numerical simulation plays a fundamental role in the results obtained. As an example, we show the results of integrating the two sets in the parameter region $0.0062 \leq k \leq 0.0072$, and $0 \leq \varepsilon \leq 0.1$. In this region, attractors A and B are complicated attractors and their dynamics are best visualized using the Poincaré section technique [18], which consists of investigating, instead of the complete trajectory, only the intersection points of the trajectory with a two-dimensional plane. Here we plot the transversal cut of the attractor with the plane $N = N_{\rm th}$ on the plane formed by the normalized intensity $I(t)/I_{\rm sol}$, and the phase delay $\phi(t) - \phi(t-\tau)$. The results obtained are arranged in a matrix; the columns correspond to Poincaré sections that have equal ε and increasing k, while the rows correspond to Poincaré sections that have equal k and increasing ε.

Fig. 3 shows the results obtained integrating set 1, while Fig. 4 shows the results obtained integrating set 2. The trajectories originated from initial conditions in modes A and B are plotted together in order to illustrate the parameter regions where the attractors A and B coexist.

The Poincaré section located in the upper left corner of Fig. 3 ($k = 0.0062$, $\varepsilon = 0$) is the transversal cut of the trajectory shown in Fig. 1(a) with the plane $N = N_{\rm th}$, and indicates that attractor A is a torus that period-doubled at a lower feedback level. Also, the Poincaré section located in the lower left corner of Fig. 3 ($k = 0.0072$, $\varepsilon = 0$) is the transversal cut of the trajectory shown in Fig. 2(a) and indicates that for these parameter values the trajectory switches between two different attractors.

The first columns of Figs. 2 and 3 are equal, since for $\varepsilon = 0$ sets 1 and 2 are equal. Clearly, the results obtained in the rest of the colums are very different; the sections of the attractors and the effect of the parameter differ strongly. In the dynamics of set 1, the effect of increasing ε is opposite to the effect of increasing k. Notice in Fig. 3 that when ε increases attractors A and B recover stability and undergo inverse period-doubling bifurcations. On the contrary, in the dynamics of set 2, there are parameter regions where the effect of ε on the Poincaré sections of the attractors is similar to the effect of k. For example, notice that in Fig. 4 for $k = 0.0072$, $\varepsilon = 0.02$, attractor B is a limit cycle, and when ε increases the limit cycle turns into a torus that period doubles.

Also, the parameter regions where attractors coexist are different. There are parameter regions where in the dynamics of set 1 only attractor A is stable, while in the dynamics of set 2 attractors A and B are both stable (for example, for $k = 0.0064$, $\varepsilon = 0.02$ in Fig. 3, we see only attractor A, while in Fig. 4 we see attractors A and B). In addition, there are parameter regions where in the numerical simulation of set 1 attractor A is stable, while in the numerical simulation of set 2 attractor B is stable (for example, notice that for $k = 0.0066$, $\varepsilon = 0.02$ in Fig. 3 we see attractor A, while in Fig. 4 we see attractor B).

III. Discussion

In order to explain the results obtained in the previous section, in this section, we study the behavior of the modes of sets 1 and 2 when the parameter ε varies. Taking into account

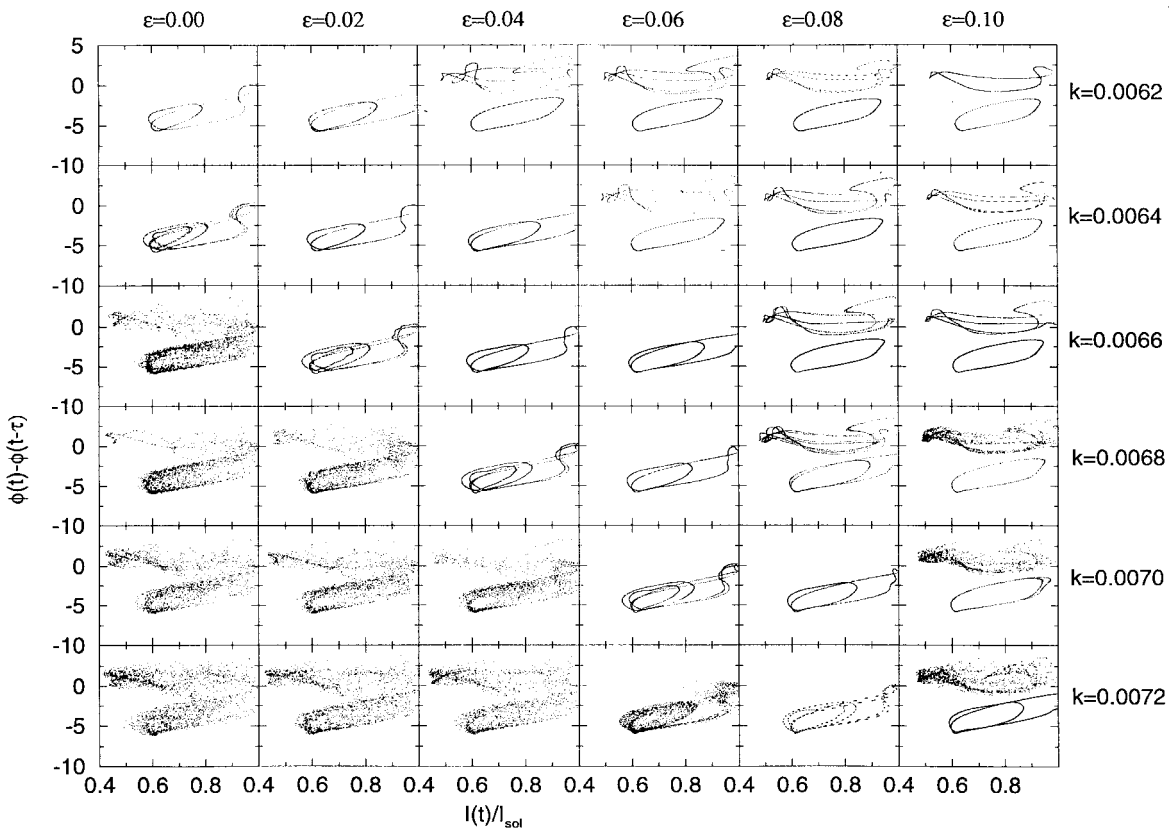

Fig. 3. Coexistence of attractors A and B in the dynamics of set 1 for $0.0062 \leq k \leq 0.0072$, and $0 \leq \varepsilon \leq 0.1$. The transversal cuts of the attractors A and B with the plane $N = N_{\rm th}$ are plotted together (for each attractor, 2000 points are shown).

gain saturation effects, the modes of set 1 satisfy (7)–(9) with $G_s = G_N(N_s - N_o)(1 - \varepsilon I_s)$ while the modes of set 2 satisfy

$$\omega_s\tau - \omega_o\tau = 1/2\alpha G_N(N_s - N_{\rm th})\tau - \gamma\tau\sin(\omega_s\tau) \quad (10)$$

[instead of (7)] and (8) and (9).

Since the phase condition (7) is independent of ε, the number of modes of set 1 and their $\omega_s\tau$ values are independent of ε. Because G_s depends on ε, the stationary field amplitude I_s and carrier density N_s of a given mode depend on ε. In the Appendix, we demonstrate that the stationary field amplitude of the modes decreases with ε, while the stationary carrier density increases with ε. The rate of variation with ε is the same for all the modes and in a very good approximation depends only on the product $G_N\tau_s$ and not on other laser parameters or external cavity parameters.

In contrast, the number of modes of set 2 and their $\omega_s\tau$ values depend on ε, since (10) can be rewritten with an explicit ε dependency as [11], [12]

$$\omega_s\tau - \omega_o\tau = \frac{\tau}{2\tau_p}\alpha'(\varepsilon)I_s(\varepsilon)\varepsilon - \gamma\tau[\alpha'(\varepsilon)\cos(\omega_s\tau) + \sin(\omega_s\tau)] \quad (11)$$

where $\alpha'(\varepsilon) = \alpha/(1 - \varepsilon I_s)$. The values of $\omega_s\tau, I_s$, and N_s of the exact stationary solutions of set 2, for $k = 0.006$ and $0 \leq \varepsilon \leq 1$, are shown in Fig. 5. Notice that although the number of modes remains approximately the same (between 5 and 7), as ε increases pairs of modes are created and destroyed.

The classification of the fixed points into modes and antimodes would require a stability analysis. However, the direct numerical simulation of set 2 shows that in the direct saddle-node bifurcations the pair of fixed points created are both unstable; one of them becomes stable when ε increases and, in the inverse saddle-node bifurcations, the pair of fixed points annihilated are one stable and one unstable.

The behavior of the modes of set 2 when ε varies explains the results found in the previous section. First, increasing ε causes the creation and annihilation of pairs of modes, and as a consecuence the value of $\Delta = \omega_s\tau$ of the modes increases with ε. Therefore, the value of Δ of the attractors originated from these modes will also increase with ε. Second, when a pair of modes is created, one of the modes is unstable and becomes stable increasing ε. Therefore, the attractor originated from this mode will be unstable and will become stable and reverse the route to chaos, increasing ε.

With the purpose of explaining the differences found integrating sets 1 and 2 for very low values of ε, we calculated the value of $\zeta(t) = -G_N(N - N_o)\varepsilon E^2$, which is the difference between $G - 1/\tau_p$ and $G_N(N - N_{\rm th})$, i.e., it is the difference between (5) and (6). It was found that although $\zeta \to 0$ when $\varepsilon \to 0$, when $\varepsilon \neq 0$ the value of $\langle\zeta\rangle$ cannot be neglected in comparison with the value of $\langle G_N(N - N_{\rm th})\rangle$. For our parameter values and $k = 0.0072, \varepsilon = 0.1$ $\langle\zeta(t)\rangle \approx -0.6$ while $\langle G_N(N - N_{\rm th})\rangle \approx 0$. The value of $\zeta(t)$, which is neglected in set 2 while taken into account in set 1, is probably the origin

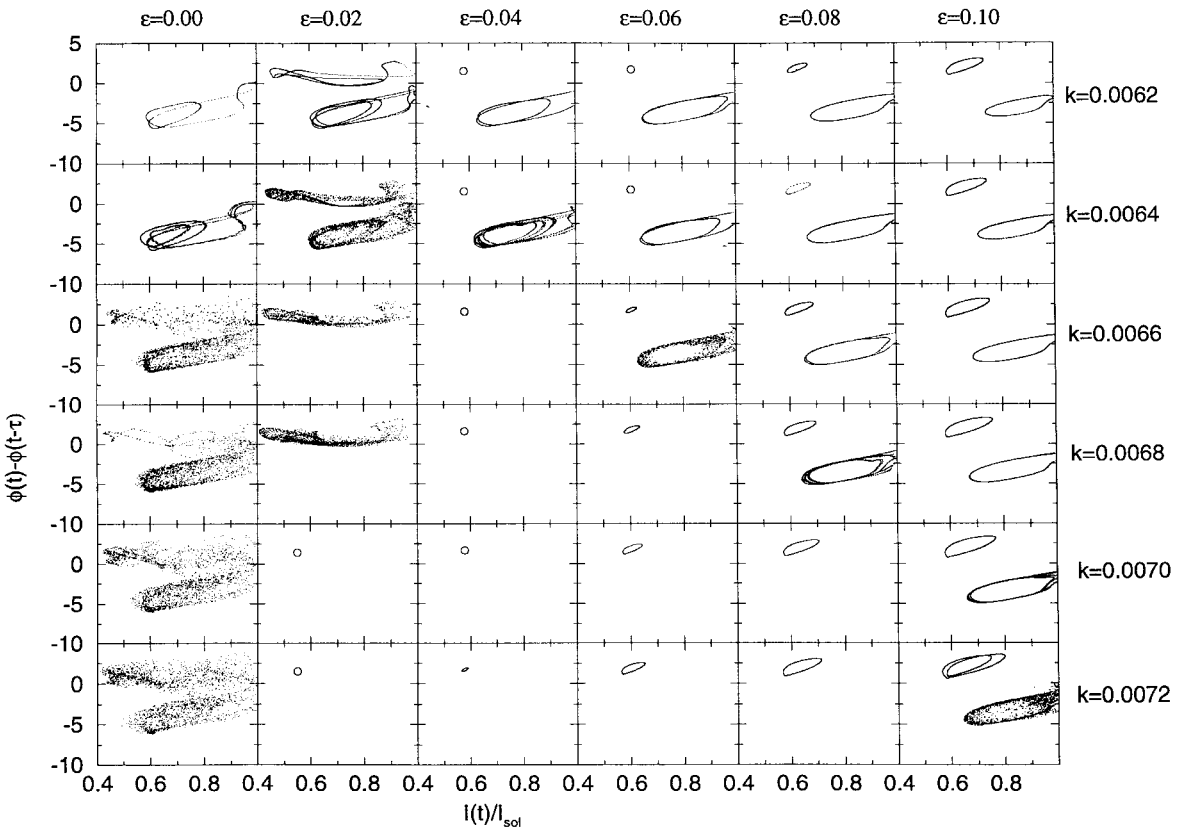

Fig. 4. Coexistence of attractors in the dynamics of set 2, for the same initial conditions and parameter values as in Fig. 3. The Poincaré section of the limit cycle originated from mode B is indicated in the figures with a small circle.

of the differences found for low values of ε in the numerical simulation of sets 1 and 2.

Finally, and in order to determine if not only the intensity dependence of G but also the intensity dependence of α has important effects on the dynamics, we numerically simulated set 1 with $\alpha = \alpha_o/(1 - \varepsilon E^2), \alpha_o$ being constant ($\alpha_o = 6$) [19]. We did not find any important difference with respect to the results obtained when $\alpha = \alpha_o$.

IV. Conclusion

In this paper, we have studied in detail the dynamics of two different versions of the Lang and Kobayashi equations for a single-mode semiconductor laser with optical feedback. The two versions are (5) and (3) (set 1) and (6) and (3) (set 2), and they differ in the way the linewidth enhancement factor α is introduced in the rate equation of the complex electric field. The two sets are equal when a linear gain is assumed, but if the nonlinear gain is taken into account, we have shown that the dynamics they predict is very different, even for low values of the gain saturation coefficient ε.

We found that the behavior of the external cavity modes, the parameter regions where two attractors coexist, and the effect of the parameter ε depend on set of equations on which the investigations are based.

In the numerical simulation of set 1, increasing the value of the parameter has a stabilizing effect in the dynamics, since it causes the attractors to reverse the route to chaos that they followed for increasing feedback. The effects of the parameters k and ε in the dynamics of set 1 are apparently opposite, and the detailed comparison between them is presented in the companion paper [20]. In the numerical simulation of set 2, in addition to causing the attractors to reverse the route to chaos, an increase of ε also causes an increase of the phase difference $\Delta(t) = \omega_o\tau + \phi(t) - \phi(t - \tau)$ of the attractors.

These results were understood by studying the behavior of the modes of sets 1 and 2 when ε varies. It was shown that the number of modes of set 1 and their $\omega_s\tau$ value are independent of ε. An increase of the value of ε causes a decrease of the stationary intensity I_s and an increase of the stationary carrier density N_s, but leaves the $\Delta = \omega_s\tau$ value of the modes unchanged.

In the dynamics of set 2, it was shown that when ε increases pairs of modes are created and destroyed via direct and inverse saddle-node bifurcations, and, as a consequence, although the number of modes remains approximately the same, their $\Delta = \omega_s\tau$ value increases with ε. Therefore, the attractors originated from these modes will have a Δ value that will increase with ε. In contrast to what occurs when k is increased, when ε is increased the pair of fixed points created are both initially unstable, but as ε increases one of the points becomes a stable mode before colliding with an antimode.

It should be noted that in the literature the investigations of laser dynamics have been based on either of the two sets of Lang and Kobayashi equations studied here. Therefore, our

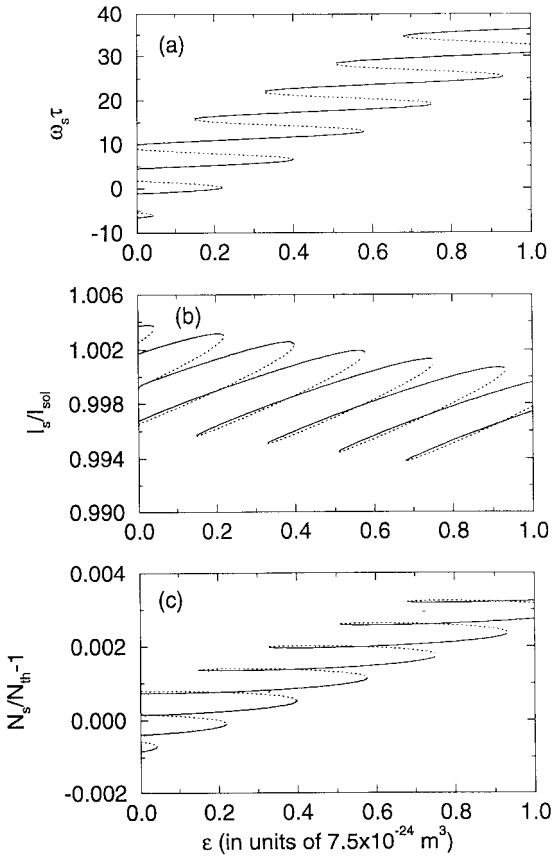

Fig. 5. Bifurcation diagram of the stationary solutions of set 2, obtained solving (10), (8), and (9) for $k = 0.006$ and $0 \leq \varepsilon \leq 1$. The dashed lines represent antimodes while the solid lines represent modes that are unstable when they are created but become stable before they disappear.

results show that if the nonlinear gain was considered, one must take into account the particular set of equations employed when interpreting the results.

An important parameter in this study in the pump factor $J/J_{\rm th}$ (where $J_{\rm th}$ is the threshold current density). The photon density E^2 in semiconductor lasers is very high, even for low output powers, because of the small cross-sectional area of the active region. Therfore, the nonlinear gain can be neglected when the laser is operated close to threshold, but nonlinear optical phenomena will occur when the laser is driven far above threshold. Therefore, we expect that the differences predicted by sets 1 and 2 would not be as relevant close to threshold as they are far above threshold (here we used $J/J_{\rm th} = 2$).

Another important parameter is the external cavity length. Semiconductor lasers are commonly employed in optical fiber communication systems, and it would be interesting to study the behavior predicted by sets 1 and 2 when the optical feedback is from a large external cavity. We speculate that the distance from the remote reflector to the laser source and the nonlinearities of the active medium should modify drastically the laser operational characteristics, since as τ increases more external cavity modes come into play. Their ω_s frequency, according to set 1, should be independent of the gain nonlinearity, while accordingly to set 2, their ω_s should present a shift that is related to the magnitude of the nonlinear gain coefficient.

Also, we expect that neglecting or taking into account the nonlinear gain in the expresion of the optical frequency ω should lead to different results when the solitary laser is operated under modulation of the injection current, or when there is external light injection from another laser. All these effects, which are very common in laser-based devices, lead to variations of photon density. Therefore, we expect nonlinear optical phenomena to play an important role and different dynamics if we asume that ω depends on the photon density than if we assume ω is photon density-independent.

APPENDIX

In this appendix, we show that the stationary intensity I_s (the stationary carrier density N_s) of the modes of set 1 decreases (increases) with the value of the parameter ε.

The values of N_s and I_s of a given mode satisfy

$$N_s(\varepsilon) = J\tau_s - G_s\tau_s I_s(\varepsilon) \tag{A1}$$

$$I_s(\varepsilon) = \{B + A\varepsilon - B\sqrt{1 + 2[(2G_s - A)/B]\varepsilon + [A^2/B^2]\varepsilon^2}\}/2B\varepsilon \tag{A2}$$

where $A = G_N(J\tau_s - N_o)$ and $B = G_N G_s \tau_s$. Since for set 1 the value of $\omega_s\tau$ of a given mode is independent of ε, the value of $G_s = G_N(N_s - N_o)(1 - \varepsilon I_s) = 1/\tau_p - 2\gamma\cos(\omega_s\tau)$ is also independent of ε. Expanding the square root to second-order in ε, we obtain

$$I_s(\varepsilon) = \frac{A - G_s}{B} - \frac{G_s(A - G_s)}{B^2}\varepsilon \tag{A3}$$

$$N_s(\varepsilon) = N_o + \frac{G_s}{G_N} + \frac{A - G}{G_N^2\tau_s}\varepsilon. \tag{A4}$$

If the nonlinear gain is neglected, N_s and I_s satisfy $I_s(0) = (A - G_s)/B, N_s(0) = N_o + G_s/G_N$. Therefore,

$$I_s(\varepsilon) = I_s(0)\left[1 - \frac{\varepsilon}{G_N\tau_s}\right] \tag{A5}$$

$$N_s(\varepsilon) = N_s(0)\left[1 + \sigma\frac{\varepsilon}{G_N\tau_s}\right] \tag{A6}$$

where

$$\sigma = \frac{(a-1)G_N N_o + (a-1)/\tau_p + 2\gamma\cos(\omega_s\tau)}{G_N N_o + 1/\tau_p - 2\gamma\cos(\omega_s\tau)}$$

and $a = J/J_{\rm th}$ is the pump factor. σ is a coefficient independent of ε, which for typical parameter values can be approximated as $\sigma \approx (a - 1)$. Equations (A5) and (A6) therefore show that the value of I_s of all the modes decreases with ε while the value of N_s increases with ε, and that the rate of variation with ε is the same for all the modes.

REFERENCES

[1] C. H. Henry, "Theory of the linewidth of semiconductor lasers," *IEEE J. Quantum Electron.*, vol. QE-18, pp. 259–264, 1982.

[2] G. P. Agrawal and N. K. Dutta, *Long-Wavelength Semiconductor Lasers*. New York: Van Nostrand Reinhold, 1986.

[3] R. Lang and K. Kobayashi, "External optical feedback effects on semiconductor laser properties," *IEEE J. Quantum Electron.*, vol. QE-16, pp. 347–355, 1980.

[4] B. Tromborg, J. H. Osmundsen, and H. Olesen, "Stability analysis for a semiconductor laser in an external cavity," *IEEE J. Quantum Electron.*, vol. QE-20, pp. 1023–1032, 1984.

[5] D. Lenstra, B. H. Verbeek, and A. J. den Boef, "Coherence collapse in single-mode semiconductor lasers due to optical feedback," *IEEE J. Quantum Electron.*, vol. QE-21, pp. 674–679, 1985.

[6] N. Schunk and K. Petermann, "Numerical analysis of the feedback regimes for a singe-mode semiconductor laser with external feedback," *IEEE J. Quantum Electron.*, vol. 24, pp. 1242–1247, 1988.

[7] J. S. Cohen and D. Lenstra, "Spectral properties of the coherence collapsed state of a semiconductor laser with delayed optical feedback," *IEEE J. Quantum Electron.*, vol. 25, pp. 1143–1151, 1989.

[8] J. Wang and K. Petermann, "Noise analysis of semiconductor lasers within the coherence collapse regime," *IEEE J. Quantum Electron.*, vol. 27, pp. 3–9, 1991; see also the correction in *IEEE J. Quantum Electron.*, vol. 27, p. 2365, 1991.

[9] J. MØrk, B. Tromborg, and J. Mark, "Chaos in semiconductor lasers with optical feedback: Theory and experiment," *IEEE J. Quantum Electron.*, vol. 28, pp. 93–108, 1992.

[10] J. Ye, H. Li, and J. G. McInerney, "Period-doubling route to chaos in a semiconductor laser with weak optical feedback," *Phys. Rev. A*, vol. 47, pp. 2249–2252, 1993.

[11] A. Ritter and H. Haug, "Theory of laser diodes with weak optical feedback. I. Small-signal analysis and side-mode spectra," *J. Opt. Soc. Amer. B*, vol. 10, pp. 130–144, 1993.

[12] _____, "Theory of laser diodes with weak optical feedback. II. Limit-cycle behavior, quasiperiodicity, frequency locking, and route to chaos," *J. Opt. Soc. Amer. B*, vol. 10, pp. 145–154, 1993.

[13] Y. Huang Kao, N. Ming Wang, and H. Ming Chen, "Mode description of routes to chaos in external-cavity coupled semiconductor lasers," *IEEE J. Quantum Electron.*, vol. 30, 1732–1739, 1994.

[14] V. Annovazzi-Lodi, S. Donati, and M. Manna, "Chaos and locking in semiconductor lasers due to external injection," *IEEE J. Quantum Electron.*, vol. 30, pp. 1537–1540, 1994.

[15] J. Dellunde, M. C. Torrent, C. R. Mirasso, E. Hernandez-Garcia, J. M. Sancho, "Analytical calculations of switch-on time and timing jitter in diode lasers subjected to optical feedback and external light injection," *Opt. Commun.*, vol. 115, pp. 523–527, 1995.

[16] C. Masoller, C. Cabeza, and A. C. Sicardi Schifino, "Study of the effect of the nonlinear gain in the visibility of a semiconductor laser with incoherent feedback in the coherence collapsed regime: theory and experiment," *IEEE J. Quantum Electron.*, vol. 31, pp. 1022–1029, 1995.

[17] C. Masoller, "Coexistence of attractors in a laser diode with optical feedback from a large external cavity," *Phys. Rev. A*, vol. 50, pp. 2569–2579, 1994.

[18] H. G. Schuster, *Deterministic Chaos*, 2nd. ed. Weinheim, Germany: VCH, 1988.

[19] G. P. Agrawal, "Intensity dependence of the linewidth enhancement factor and its implications for semiconductor lasers," *IEEE Photon. Technol. Lett.*, vol. 1, pp. 212–214, 1989.

[20] C. Masoller, "Comparision of the effects of nonlinear gain and weak optical feedback on the dynamics of semiconductor lasers," this issue, pp. 804–814.

C. Masoller, photograph and biography not available at the time of publication.